Resource

Cell Reports

Elucidating the Neuronal Architecture of Olfactory Glomeruli in the *Drosophila* Antennal Lobe

Graphical Abstract

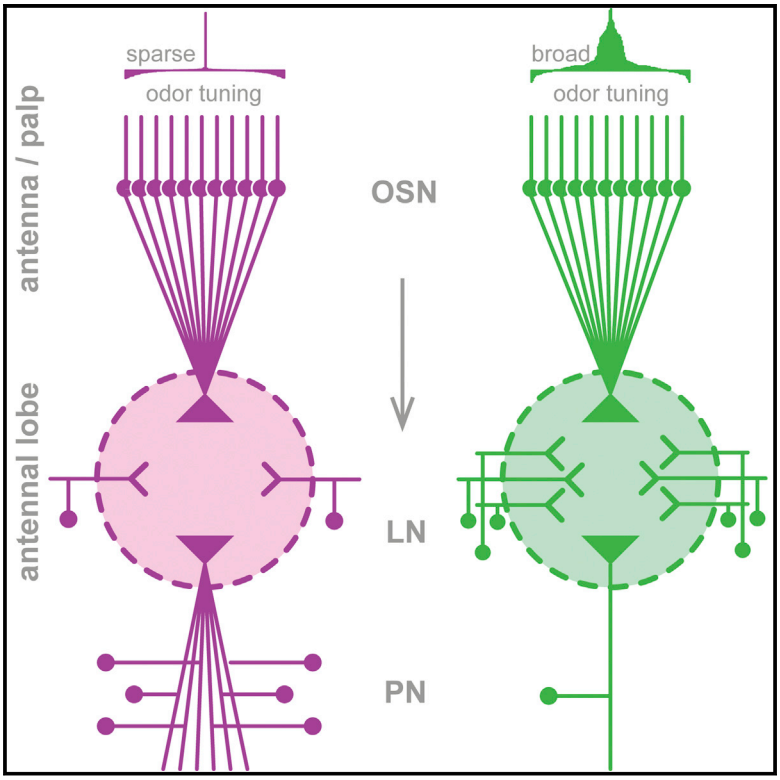

Authors

Veit Grabe, Amelie Baschwitz, Hany K.M. Dweck, Sofia Lavista-Llanos, Bill S. Hansson, Silke Sachse

Correspondence

ssachse@ice.mpg.de

In Brief

Olfactory glomeruli, functional units of advanced olfactory systems, are usually expected to share a common morphology. However, Grabe et al. demonstrate in Drosophila melanogaster that the neuronal architecture of each glomerulus is unique and reflects its behavioral relevance.

Highlights

- The neuronal composition of glomeruli is unique
- Glomerular volume is determined largely by the number of olfactory sensory neurons
- Selectivity of a glomerulus is represented by the number of second-order neurons
- Glomeruli encoding crucial odors possess a large number of PNs and low LN innervation

Grabe et al., 2016, Cell Reports *16*, 3401–3413
September 20, 2016 © 2016 The Author(s).
http://dx.doi.org/10.1016/j.celrep.2016.08.063

Cell Reports
Resource

OPEN ACCESS
CellPress

Elucidating the Neuronal Architecture of Olfactory Glomeruli in the *Drosophila* Antennal Lobe

Veit Grabe,[1,3] Amelie Baschwitz,[1,3] Hany K.M. Dweck,[1,2] Sofia Lavista-Llanos,[1] Bill S. Hansson,[1] and Silke Sachse[1,4,*]
[1]Department of Evolutionary Neuroethology, Max Planck Institute for Chemical Ecology, Hans-Knöll-Strasse 8, 07745 Jena, Germany
[2]Present address: Department of Molecular, Cellular, and Developmental Biology, Yale University, New Haven, CT 06520, USA
[3]Co-first author
[4]Lead Contact
*Correspondence: ssachse@ice.mpg.de
http://dx.doi.org/10.1016/j.celrep.2016.08.063

SUMMARY

Olfactory glomeruli are morphologically conserved spherical compartments of the olfactory system, distinguishable solely by their chemosensory repertoire, anatomical position, and volume. Little is known, however, about their numerical neuronal composition. We therefore characterized their neuronal architecture and correlated these anatomical features with their functional properties in *Drosophila melanogaster*. We quantitatively mapped all olfactory sensory neurons (OSNs) innervating each glomerulus, including sexually dimorphic distributions. Our data reveal the impact of OSN number on glomerular dimensions and demonstrate yet unknown sex-specific differences in several glomeruli. Moreover, we quantified uniglomerular projection neurons for each glomerulus, which unraveled a glomerulus-specific numerical innervation. Correlation between morphological features and functional specificity showed that glomeruli innervated by narrowly tuned OSNs seem to possess a larger number of projection neurons and are involved in less lateral processing than glomeruli targeted by broadly tuned OSNs. Our study demonstrates that the neuronal architecture of each glomerulus encoding crucial odors is unique.

INTRODUCTION

Species of divergent animal phyla with advanced olfactory systems share an important feature: all develop olfactory glomeruli (Strausfeld and Hildebrand, 1999). During recent decades, the wiring properties of these spherical compartments have been elucidated in great detail in the mammalian olfactory bulb as well as in the insect antennal lobe (AL) (Hansson et al., 2010; Mombaerts, 2006; Vosshall and Stocker, 2007; Wilson, 2013; Wilson and Mainen, 2006). In spite of this, little is known about the numerical neuronal composition of individual glomeruli. Given that different glomeruli do not accomplish uniform tasks, their neuronal architecture should not be homogeneous. Many studies in *Drosophila* provide evidence that each glomerulus represents a specific coding channel determined by the odor response profile of the olfactory receptor expressed by the innervating sensory neuron type (Ai et al., 2010; Dweck et al., 2015; Ebrahim et al., 2015; Hallem and Carlson, 2006; Kreher et al., 2008; Kurtovic et al., 2007; Ronderos et al., 2014; Silbering et al., 2011; Stensmyr et al., 2012; Suh et al., 2004). In order to determine whether each individual glomerulus represents indeed a unique structural coding unit, we characterized the complete neuronal architecture of each individual glomerulus of the *Drosophila* AL. Furthermore, we correlated these anatomical features with their functional properties. We used the genetic model organism *Drosophila melanogaster* because the different neuronal populations of the AL have been anatomically and functionally well characterized (Stocker et al., 1990) and can be selectively labeled and analyzed. In addition, a significant amount of data regarding specific odor-driven behavior has been produced lately (Duménil et al., 2016; Ebrahim et al., 2015; Grosjean et al., 2011; Knaden et al., 2012; Semmelhack and Wang, 2009; Stensmyr et al., 2012).

Olfactory sensory neurons (OSNs), in *Drosophila*, are housed in four different sensillum classes present on the third antennal segment and on the maxillary palp (Shanbhag et al., 1999) (Figures 1A and 1A′). Each OSN expresses one, in some instances two, specific olfactory receptors (Benton et al., 2009; Couto et al., 2005; Fishilevich and Vosshall, 2005). OSNs expressing the same olfactory receptor converge on one of the 52 glomeruli of the AL (Gao et al., 2000; Grabe et al., 2015; Vosshall et al., 2000) (Figure 1A″). The AL represents the first olfactory center and conveys odor-induced activity patterns via projection neurons (PNs) to the protocerebrum (Vosshall and Stocker, 2007), where the olfactory information is integrated with other sensory modalities. OSNs synapse within each glomerulus of the AL via defined synapse numbers (Mosca and Luo, 2014) with most of the PNs and multiglomerular local interneurons (LNs) (Chou et al., 2010; Rybak et al., 2016; Seki et al., 2010). As mentioned above, several studies have characterized the molecular receptive range of most olfactory receptors and have thus provided us with a nearly complete functional characterization of the odor-tuning properties of OSNs targeting each glomerulus, which are accessible through

This is an open access article under the CC BY-NC-ND license (http://creativecommons.org/licenses/by-nc-nd/4.0/).

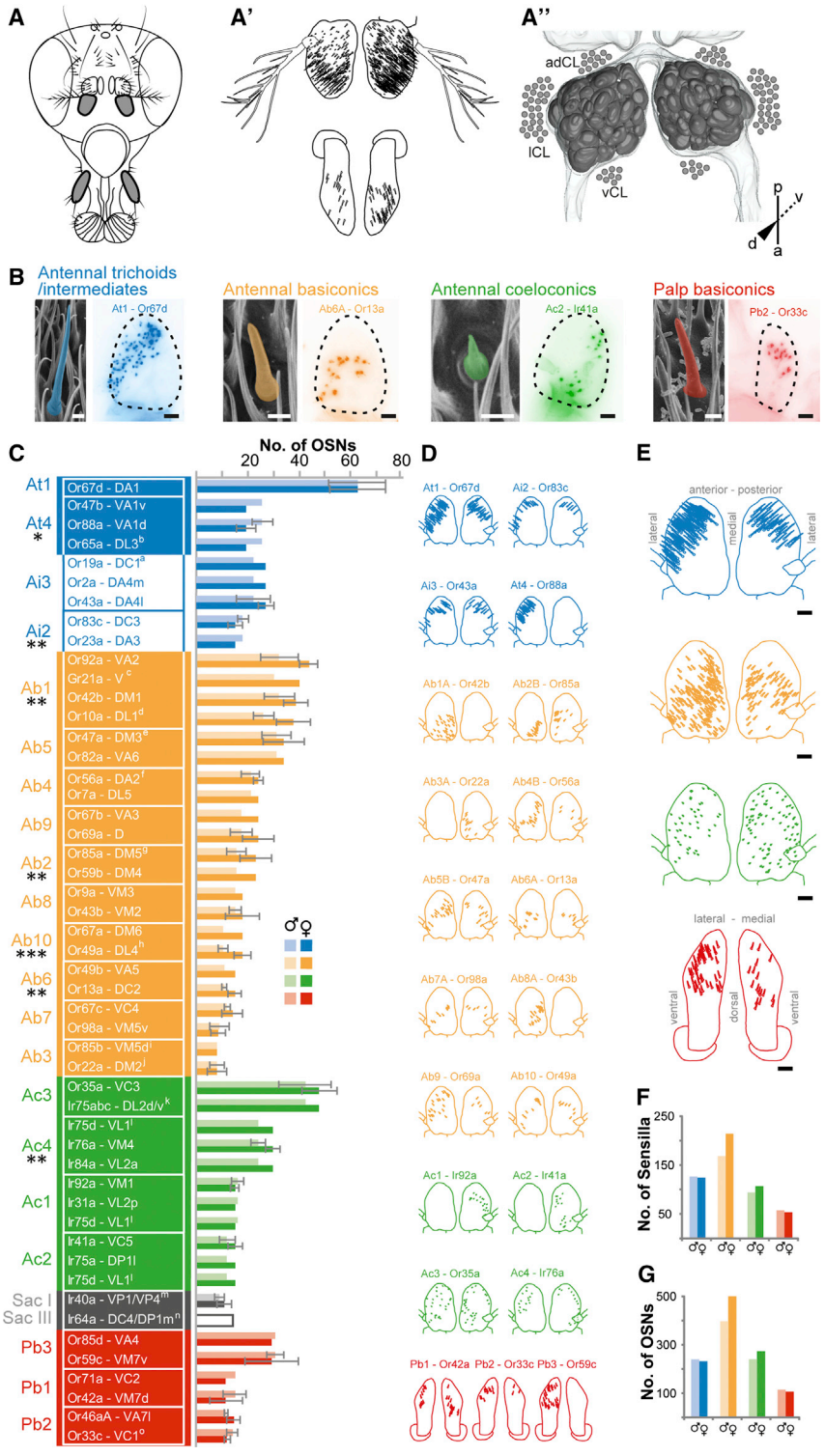

Figure 1. Each Glomerulus Receives Input from a Specific Number of OSNs

(A) Schematic of the *Drosophila* head in frontal view. The third antennal segments and maxillary palps—the major olfactory organs—are highlighted in gray and enlarged in (A′) (same perspective). (A′′) The antennal lobes, primary olfactory center in the brain, in dorsal view, including the three soma clusters (adCL, anterodorsal cluster; lCL, lateral cluster; vCL, ventral cluster).

(B) Electron microscopic scans of each sensillum class (left) and representative olfactory receptor mappings of the four sensillum classes (right). The scale bar in the scanning electron micrographs represents 2 μm; the scale bar in the fluorescence images represents 20 μm.

(C) Number of OSNs for each olfactory receptor and sensillum type. OSN numbers were acquired by quantifying at least one OSN type per sensillum type in males and females (indicated by error bars). Number of OSNs expressing Gr21a represents the mean of all counted Ab1 OSNs. Data represent median ± SD. Statistical differences between sexes were determined by Student's t test (*$p < 0.05$, **$p < 0.01$, ***$p < 0.001$; n = 5–30). Colors indicate the different sensilla classes as shown in (B). Data from males and females are shown by light (male) and dark (female) colors. [a]Coexpressing Or19b; [b]coexpressing Or65b and Or65c; [c]coexpressing Gr63a; [d]coexpressing Gr10a; [e]coexpressing Or33b; [f]coexpressing Or33a; [g]coexpressing Or33b; [h]coexpressing Or85f; [i]coexpressing Or98b; [j]coexpressing Or22b; [k]after Silbering et al. (2011): both parts of DL2 receive putative input from Ir75abc in Ac3; [l]after Silbering et al. (2011): receiving input from Ac1, Ac2 and Ac3; [m]data from Kain et al. (2013); [n]data from Ai et al. (2010); [o]coexpressing Or85e.

(D) Distribution of single sensillum types on the female antenna and palp.

(E) Distribution of all counted sensilla according to class. The scale bar represents 20 μm.

(F) Sex-specific differences of sensillum number per class.

(G) Sex-specific differences of OSN number per sensillum class.

the DoOR database (Galizia et al., 2010). Notably, several of these olfactory receptor types mediate information regarding unique and behaviorally highly relevant odors, such as sexual pheromones (Dweck et al., 2015; Ha and Smith, 2006; Kurtovic et al., 2007), oviposition cues (Dweck et al., 2013) and strongly aversive odors that signal stress (Suh et al., 2004), or unsuitable feeding and breeding sites (Ai et al., 2010; Ebrahim et al., 2015; Stensmyr et al., 2012). Beyond these functional differences, each glomerulus has a unique shape and size (Grabe et al., 2015; Laissue et al., 1999), suggesting that the number and composition of the innervating neurons are specific. This assumption is further supported by recent studies showing a diversified neurotransmitter repertoire in the AL (Busch et al., 2009; Carlsson et al., 2010; Liu and Wilson, 2013), as well as glomerulus-specific differences in the sensitivity to lateral inhibition (Hong and Wilson, 2015).

In the present study, we undertook a complete quantitative mapping of all receptor-specific OSNs and uniglomerular PNs that innervate each glomerulus, including sexually dimorphic distributions and glomerular volumes. By correlating these morphological features with functional properties, we provide evidence for a unique neuronal architecture of glomeruli encoding crucial odors.

RESULTS

Complete Quantitative Mapping of OSN Innervation

Although it has been shown that OSNs expressing a certain olfactory receptor occur in varying numbers, a uniform convergence of about 30:1 OSNs for each glomerulus has so far been assumed (Stocker, 2001; Vosshall and Stocker, 2007). This is because numerical OSN data have been available for only a limited set of olfactory receptor types (Dobritsa et al., 2003; Gao et al., 2000; Sachse et al., 2007). In order to determine the precise input convergence for all glomeruli in the *Drosophila* AL (Figure 1A″), we mapped and quantified the number of OSNs that express a certain olfactory receptor using specific *ORx-/IRx-GAL4* driver lines. In order to validate our methodological approach, we mapped the topographical distribution of sensilla on the antenna and the palp. To achieve this, we selected at least one OSN type per sensillum type, which has been described to be representative (Couto et al., 2005; Silbering et al., 2011) (Figures 1B and 1D). We observed a pattern of distribution of the different sensillum classes that confirmed what was previously found using single-sensillum recordings (de Bruyne et al., 1999, 2001) as well as immunohistochemistry (Fishilevich and Vosshall, 2005; Silbering et al., 2011). Moreover, our observed patterns of OSN types corresponds well with in situ hybridization data for specific OR and IR genes (Benton et al., 2009; Vosshall et al., 2000), confirming that our approach of labeling OSN types is reliable. Finally, our total numbers of the different sensillum classes for the antenna and the maxillary palps (Figures 1F and 1G) match well published data as further described below (de Bruyne et al., 2001; Shanbhag et al., 1999; Stocker, 2001).

In general, the basiconic sensilla were located almost everywhere on the third antennal segment, with higher density in the anterior proximal region; none were present at the distal tip (Figure 1E). The trichoid sensilla were located more distally, including the two intermediate types Ai2 and Ai3 (Dweck et al., 2013), which we still assigned to the trichoid sensillum group for simplicity. Coeloconic sensilla were evenly distributed with higher density at the posterior side. The basiconic sensilla on the maxillary palp were also evenly spread at the distal region of this appendage.

Next, we quantified the number of OSNs expressing each olfactory receptor type by counting at least one type per sensillum in males and females (Figure 1C; Table S1). For the number of sensory neurons in the different sacculus chambers (i.e., invaginations in the third antennal segment), we consulted recent studies (Ai et al., 2010; Kain et al., 2013). The remaining sensilla represent poreless hygro- or thermosensors (Gallio et al., 2011; Shanbhag et al., 1995) and were not included in our study. We observed OSN numbers ranging from 10 up to 65 per functional sensillum type; as an extreme example, Or67d, housed in the At4 sensillum, was expressed in the largest number of OSNs. As expected, the male antenna exhibited significantly more At4 sensilla than the female, because these sensilla house fruitless-positive OSNs and are involved in courtship behavior (Dweck et al., 2015; Kurtovic et al., 2007; Stockinger et al., 2005). Several other sensillum types, all of which were *fruitless* negative, were also present in sexually dimorphic numbers, occurring significantly more frequently in females than in males (Ab1, Ab2, Ab6, Ab10, and Ac4) or vice versa (Ai2; Figure 1C). Regarding the number of OSNs on the maxillary palps, we did not observe a clear sexual dimorphism, confirming previous studies (Stocker, 2001). Finally when we determined the total count of OSNs and sensilla on the antenna and the palp (Figures 1F and 1G), we observed that males had marginally more trichoid sensilla than females, while basiconic and coeloconic sensilla occured more frequently in females, as described earlier (Stocker, 2001).

We found a total of 417 ± 89 (average ± SD) sensilla per antenna and 57 ± 14 sensilla per palp housing 945 ± 201 and 113 ± 28 OSNs, respectively. These numbers are in line with former studies counting approximately 440 sensilla on the antenna and 60 on the palps, which house about 1,150 and 120 OSNs, respectively (Stocker, 2001). In order to verify whether our quantification with specific *ORx-/IRx-GAL4* lines is comprehensive, we labeled all OSNs on the maxillary palp by expressing the nuclear marker nls-GFP using the *Orco-Gal4* driver line (Larsson et al., 2004), as well as all coeloconic sensilla on the antenna via the *Ir8a-GAL4* line (Silbering et al., 2011). We counted 100 ± 4 (average ± SD) Orco-expressing OSNs on the maxillary palp and 130 ± 21 Ir8a-expressing OSNs on the antenna (n = 3–7 female flies). These numbers match reasonably well our specific quantifications for female flies, which resulted in 108 ± 19 OSNs on the palp and 107 ± 14 coeloconic sensilla on the antenna and confirms the reliability of our quantitative approach. Unfortunately, we could not reliably quantify the number of Orco-expressing OSNs on the antenna, becasue Orco is heterogeneously expressed in the different sensilla classes with high expression levels in the basiconic sensilla and low levels in the trichoids (Benton et al., 2006; Larsson et al., 2004). Because the maxillary palp has only basiconic sensilla, Orco is homogeneously expressed in all OSNs on this olfactory organ and could be used for reliable quantification.

The Number of OSNs Likely Determines Glomerular Volume

We next analyzed whether the number of olfactory input neurons correlates with the glomerular volume, as has been recently shown for a subset of glomeruli in the mouse olfactory bulb (Bressel et al., 2016). We therefore extended our previously published volumetric data set and obtained in vivo volume measurements for all glomeruli in males and females using the in vivo neuropil labeling via END1-2 (Grabe et al., 2015) (Figures 2A and 2E; Table S1; see Experimental Procedures for details). In order to adjust for inter-individual variability and sex-specific differences (Figure 2B), we compared the glomerular volume relative to the size of the summed glomerular volume per animal. We observed, for example, that glomeruli that receive input from trichoid sensilla account for about 20% or 25% of the complete AL

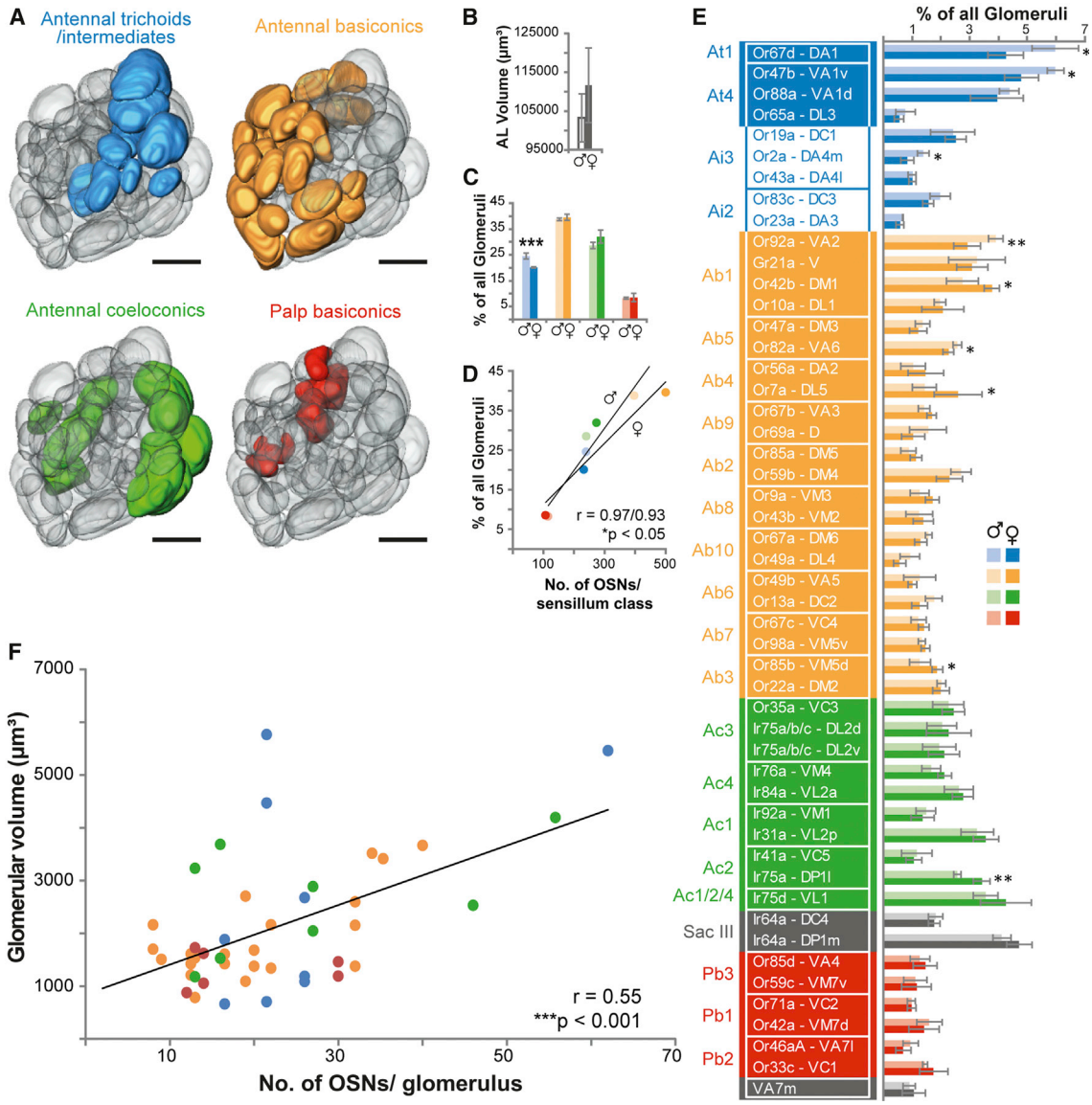

Figure 2. In Vivo Glomerular Volume Is Likely Determined by OSN Number

(A) Three-dimensional reconstructed ALs representing glomeruli separately for each class of sensillum of the corresponding OSN class. The scale bar represents 20 μm.

(B) Entire AL volume of males (empty column) and females (filled column). Data represent median ± SD.

(C) Percentage of AL volume of glomeruli innervated by each sensillum class separately in males and females. The colors indicate the sensillum classes as shown in Figure 1B. Data from males and females are indicated by light (male) and dark (female) colors. Statistical differences between sexes were determined by Student's t test (***$p < 0.001$).

(D) Correlation of OSN number per sensillum class and the respective glomerular volume for males and females (*$p < 0.05$, two-tailed probability of the Pearson correlation coefficient).

(E) Glomerulus-specific volumes shown as percentages of all labeled glomeruli per specimen. Data in (B), (C), and (E) represent median ± SD. Statistical differences between sexes were determined by Student's t test (*$p < 0.05$, **$p < 0.01$, ***$p < 0.001$; n = 4 for males and females each).

(F) Correlation of glomerular volume and OSN number (***$p < 0.001$, two-tailed probability of the Pearson correlation coefficient).

The color code refers to Figure 1B.

volume in females or males, respectively (Figure 2C). This volumetric proportion corresponds well to the proportion of OSNs expressing olfactory receptors housed in trichoid sensilla (23% in females and 26% in males). Extending this comparison to the remaining classes of sensilla, we observed a significant but shallow correlation between glomerular volume and OSN number (Figure 2D) that was also evident when we considered each glomerulus separately (Figure 2F). Hence, our data indicate

that the number of OSNs plays a role in determining glomerular volume.

Because we observed sex-specific differences for some OSN types, we wondered whether these differences become evident also in the volume of the target glomerulus. Sexual dimorphism in glomerular volume has so far been studied only for glomeruli that are involved in pheromone processing; glomeruli DA1 and VA1v, which encode the sexual pheromones *cis*-vaccenyl acetate and methyl laurate (Dweck et al., 2015; Kurtovic et al., 2007), are significantly larger in males than in females (Kondoh et al., 2003). Our volume measurements confirmed this finding and extended the list by several other glomeruli. Notably, we also observed gender-specific differences in glomeruli DA4m, VA2, and VA6, all of which are larger in males than in females, as well as in glomeruli DM1, DL5, DP1l, and VM5d, being larger in females than in males (Figure 2E; Table S1). For glomeruli VA1v and DM1, we also observed a dimorphic OSN quantity (Figure 1C). However, a sex-specific difference in glomerular volume was not always linked to a sex-specific difference in number of OSNs, implying that sensory input is the major, but not the only determinant of glomerular volume.

The Number of Excitatory Output Neurons Is Glomerulus Specific

Having shown that each glomerulus is targeted by a specific number of OSNs and that this number is correlated to the glomerular volume, we next asked whether each glomerulus is also innervated by a glomerulus-specific number of PNs. To quantify the number of output neurons for each glomerulus, we focused on uniglomerular, excitatory PNs by expressing photoactivatable GFP (Patterson and Lippincott-Schwartz, 2002) under the control of the enhancer trap line *GH146-GAL4* (Stocker et al., 1997) (Figure 3A). This line is described to label about 66% of total PNs (Stocker et al., 1997); these PNs project mainly via the medial AL tract (Ito et al., 2014) to the mushroom body calyx and farther, to the lateral horn (LH). A small proportion projects via the lateral AL tract to the LH and farther to the mushroom body calyx. Most GH146-positive PNs (i.e., 94%) are cholinergic (Shang et al., 2007). We applied repeated photoactivation of each labeled glomerulus in a minimum of three animals to gain a reliable estimate of the variability. When we quantified the excitatory output of all glomeruli that are labeled by *GH146-GAL4*, we observed two classes of glomeruli: the majority (i.e., 83%) is innervated by on average 2 ± 1 uniglomerular PNs, while the remaining glomeruli, which comprise glomeruli D, DA1, DA2, DC3, DL3, and VA1v, are innervated by on average 6 ± 2 PNs (Figure 3B; Table S1). Furthermore, we assigned each individual PN soma to the dorsomedial, lateral, or ventral cell cluster, revealing that a few glomeruli are innervated by PNs originating from more than one cluster, as described previously (Marin et al., 2002) (Table S2).

Infrequently, we also labeled one multiglomerular PN following photoactivation of some glomeruli. This PN belongs to the vPN group and it is described to innervate the entire AL (Marin et al., 2002). Possibly we do not label this vPN reliably because of its described sparse innervation in single glomeruli. Because we focused our study on uniglomerular PNs, we excluded this vPN from our quantification.

Since the *GH146-GAL4* line does not cover all uniglomerular and excitatory PNs in the AL (Lai et al., 2008), we might have underestimated the number of PNs per glomerulus. We therefore attempted to label all AL neurons by expressing photoactivatable GFP under the control of the pan-neuronal driver *elav*. However, because the cell bodies of PNs and LNs are located in the same cell clusters, labeled cell bodies could not be unambiguously assigned to PNs (data not shown). We therefore chose a different approach and quantified the number of all cholinergic uniglomerular PNs per glomerulus using the *ChA-GAL4* driver line (Salvaterra and Kitamoto, 2001) (Figure S1A). For this purpose, we photoactivated PNs in 28 glomeruli which were characterized either by being sparsely or densely innervated or by being GH146-negative (Grabe et al., 2015) (Figure S1B). Our analysis of all cholinergic PNs confirmed that our quantification of PNs per glomerulus was largely correct, except in six cases: we labeled one to three more uniglomerular PNs in the anterodorsal and lateral cell clusters in glomeruli VA1v, DA2, D, DM5, VM2, and DM6 using the enhancer trap line *GH146-GAL4* than we labeled using the *ChA-GAL4* line.

Interestingly, when we correlated glomerulus-specific PN quantities to the glomerular volume, a weak, but significant, correlation was visible (Figure 3C). Hence, uniglomerular PNs do have an impact on glomerular volume, although they have less impact than do the input neurons.

LN Innervation Is Lowest in Glomeruli Innervated by Trichoids

The remaining major neuronal population in the AL is represented by inhibitory and excitatory LNs. In order to quantify the glomerular innervation by LNs, we integrated a data set from Chou et al. (2010), in which most LNs had been thoroughly characterized with regard to their innervation frequency at the individual glomerular level, with our data. First, we analyzed the frequency of LN innervation related to each sensillum class (Figure 4A). Glomeruli innervated by OSNs housed in basiconic sensilla on the antenna or the palp or in coeloconic sensilla show a high LN innervation density of on average 83%, 87%, or 85%, respectively. Notably, glomeruli with OSN input from trichoid sensilla display a significantly lower LN innervation density, on average, 77% ($p < 0.05$, ANOVA followed by Tukey-Kramer multiple-comparisons test). Hence, glomerular innervation by LNs is not evenly distributed across the different sensillum types and might reflect a functional classification. Next, we analyzed whether the number of LNs contributes to the glomerular volume as observed for the OSNs and PNs, but we could not find any significant correlation (Figure 4B). Additionally, we did not observe any correlation between the LN density and the number of OSNs per glomerulus (Figure 4C). Instead, and interestingly, we found a significant negative correlation between LN density and the number of PNs (Figure 4D), indicating that glomeruli innervated by a high number of PNs receive a small number of LN dendrites.

Lifetime Sparseness Allows Linking Morphology to Function

Having quantified the three main neuronal populations for each glomerulus, we wondered whether the neuronal composition is

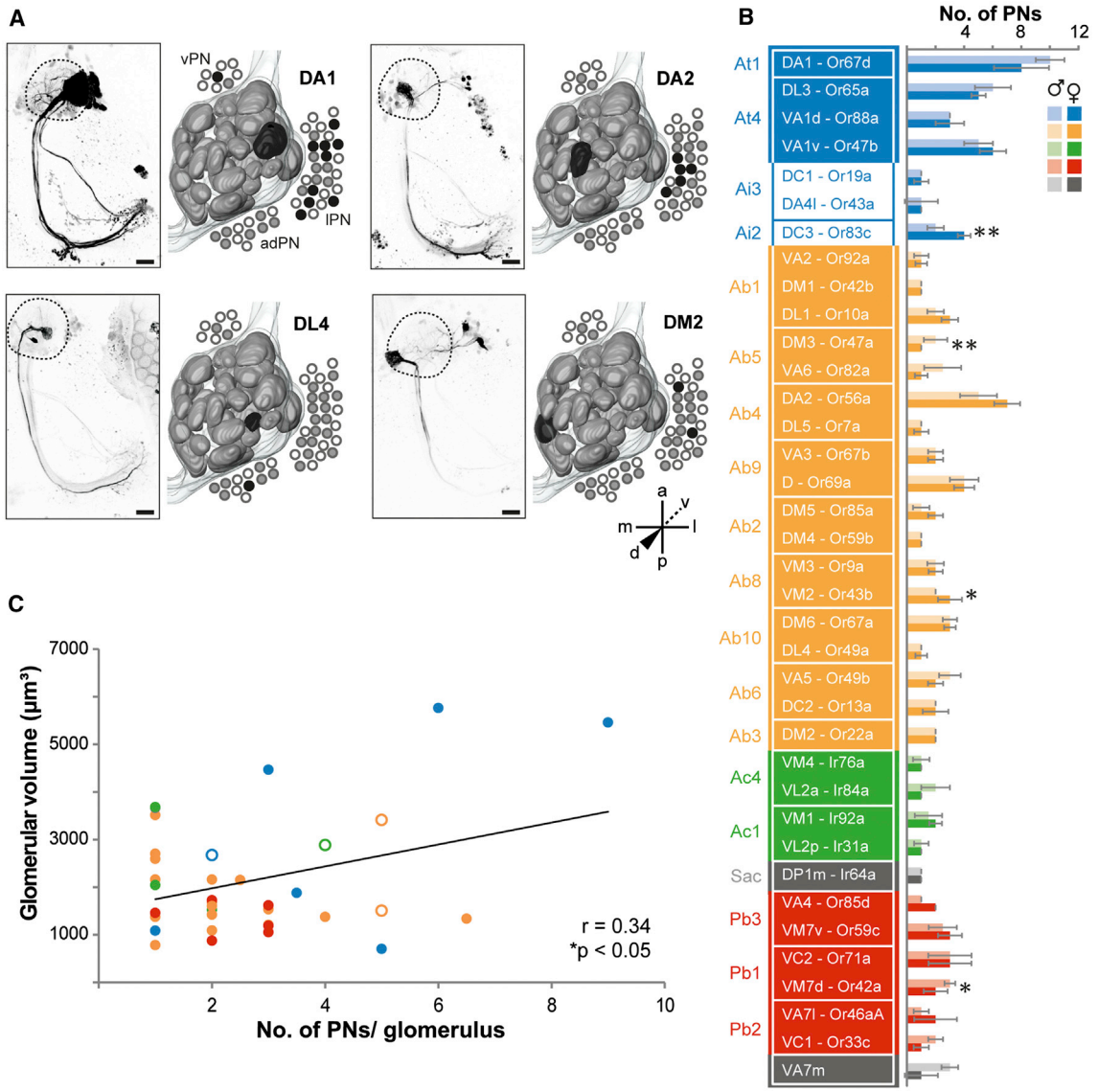

Figure 3. Number of Uniglomerular PNs per Glomerulus Is Specific

(A) Z projections of four different scans of brains expressing photoactivatable GFP in GH146-positive PNs after photoactivation of a specific glomerulus (DA1, DA2, DL4, and DM2). adPN, anterodorsal PN soma cluster; lPN, lateral PN soma cluster; vPN, ventral PN soma cluster. The scale bars represent 20 μm.

(B) Number of innervating PNs per glomerulus labeled with *GH146-GAL4;UAS-C3PA*. Data represent median ± SD. Statistical differences between sexes were determined by Student's t test (*p < 0.05, **p < 0.01; n = 3–10).

(C) Correlation of glomerular volume and PN number. Empty circles represent *ChA-GAL4;UAS-C3PA* based data (as shown in Figure S1). *p < 0.05 (two-tailed probability of the Pearson correlation coefficient).

The color code refers to Figure 1B.

reflected by the odor-tuning properties of each glomerulus. To quantify the selectivity of the response profile of a certain glomerulus, we calculated the lifetime sparseness of the olfactory receptor expressed in the OSNs innervating it (Bhandawat et al., 2007; Perez-Orive et al., 2002; Vinje and Gallant, 2000). We used the DoOR database (Galizia et al., 2010) for olfactory receptors that have been well characterized with an adequate odor set. However, several olfactory receptors have so far been tested only with a limited number of odors. In order to obtain a precise lifetime sparseness for all olfactory receptors, we extended the odor-tuning profile of 11 olfactory receptors via single-sensillum recordings (SSRs) by applying an odor set ranging from 37–474 different odors (Figure 5A; Table S3). By using our data set in addition to the odor response profiles that have already been published, we calculated the lifetime sparseness for each olfactory receptor, that is, for its corresponding glomerulus (Figure 5B; Table S1). Next, we correlated this measure to the glomerulus-specific numbers of the three main

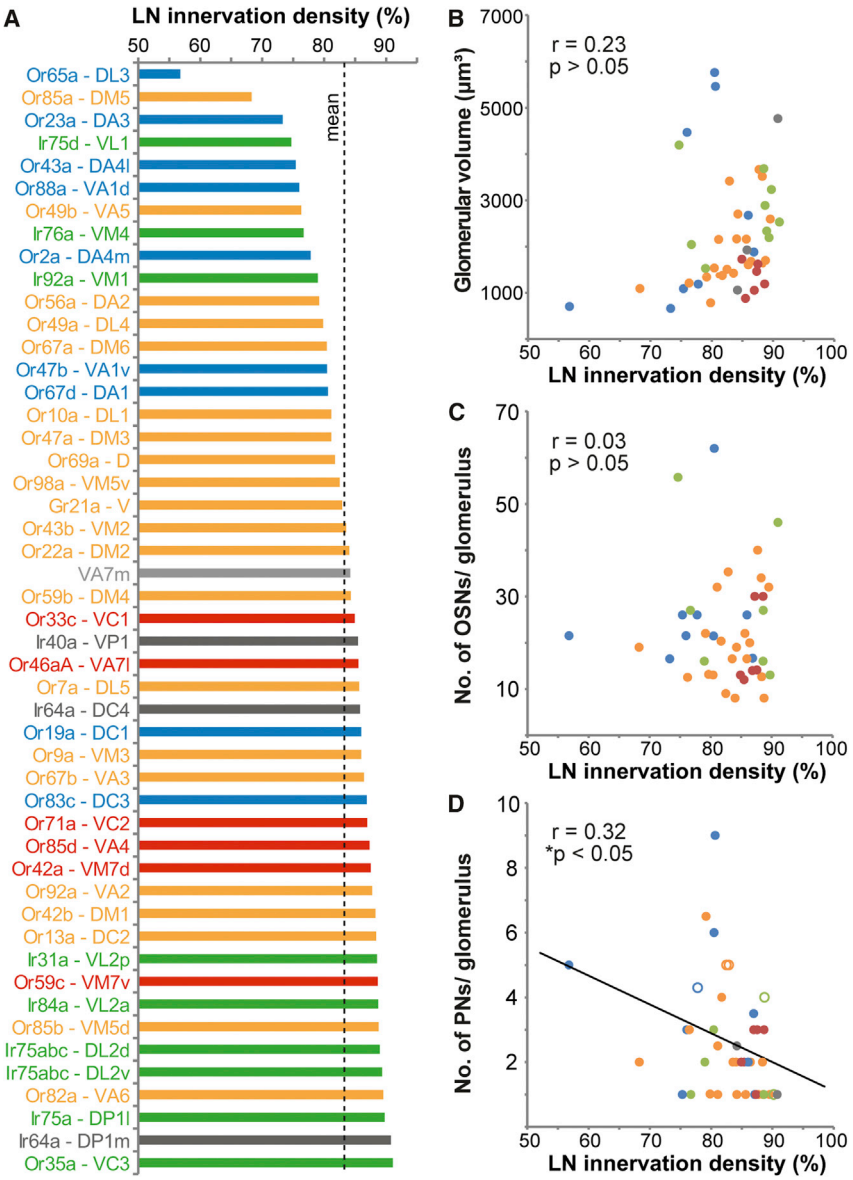

Figure 4. LN Innervation Density Is Negatively Correlated with PN Number

(A) Data set of the glomerulus-specific LN innervation frequency acquired via MARCM of several LN GAL4-Lines (data from Chou et al., 2010).

(B–D) Scatterplots representing the correlation of LN frequency with glomerular volume (B), OSN number (C), and PN number (D). *p < 0.05, two-tailed probability of the Pearson correlation coefficient.

The color code refers to Figure 1B.

neuronal populations in the AL. Although the number of OSNs does not show any correlation, we found a shallow, but significant, positive correlation with the number of PNs and a negative correlation to the LN innervation density (Figure 5C). However, because the number of PNs per glomerulus is not really continuous, the relationship between PN number and lifetime sparseness should be rather defined as two classes of glomeruli, implying that those glomeruli that have the highest sparseness seem to be innervated by more PNs than those glomeruli having a low sparseness. Hence the selectivity of a glomerulus seems to be represented not by the number of sensory input neurons innervating it but rather by the number of second-order neurons: glomeruli that are innervated by OSNs expressing a narrowly tuned olfactory receptor seem to have a higher number of PNs and are less frequently innervated by LNs, suggesting that these glomeruli perform less lateral processing. In summary, our data demonstrate that the neuronal composition of each glomerulus is specific and seems to reflect its odor-tuning profile.

DISCUSSION

Here we quantified the major neuronal populations for each individual glomerulus in the *Drosophila* AL. Using the functional characterization of a variety of olfactory receptors, our study demonstrates a correlation between functional specification and neuronal architecture. In recent decades, several neuroanatomical studies have investigated the pheromone system of several insect species; each study links a striking morphology to a specific function (Boeckh and Tolbert, 1993; Galizia et al., 1999; Hansson et al., 1992; Schneiderman et al., 1986). These studies provided evidence that the size of a glomerulus reflects its behavioral relevance. In addition, the volume of particular glomeruli in different drosophilids has been shown to be related to sensory specialization (Dekker et al., 2006; Linz et al., 2013). An enlargement in glomerular volume is correlated with either an increased number of total OSNs (Bressel et al., 2016) or an increase in their synapse number (Acebes and Ferrús, 2001). Indeed, recent ultrastructural studies have revealed that each OSN contributes an equal but specific number of synapses to a glomerulus (Mosca and Luo, 2014). In addition, it has long been known that different glomeruli receive input from various OSN numbers (de Bruyne et al., 2001; Shanbhag et al., 1999). However, the exact number of OSNs has been published only for very few olfactory receptor types so far (Dobritsa et al., 2003; Gao et al., 2000; Sachse et al., 2007). Our comprehensive OSN quantification shows that the volume of each glomerulus is most likely dictated by the number of OSNs and confirms a recent study in mice (Bressel et al., 2016). In addition, our data provide evidence that glomerular volume is also slightly correlated with the number of uniglomerular PNs.

We were able to precisely map 95% of sensillum classes and types by using 21 *OR-/IR-specific GAL4-lines* (Fishilevich and

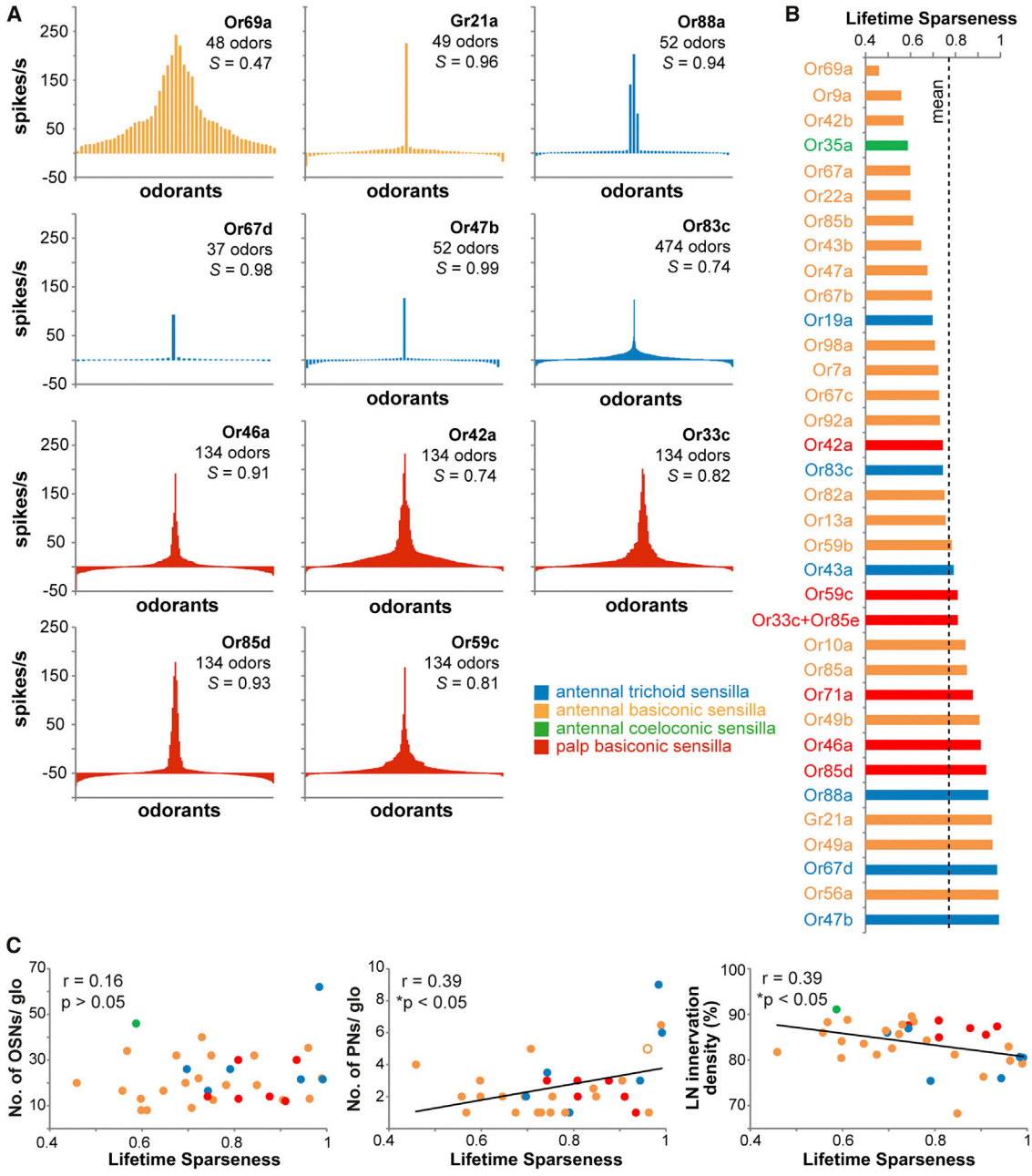

Figure 5. Odor-Tuning Properties Are Correlated with the Number of LNs and PNs per Glomerulus

(A) Odor response profiles of 11 olfactory receptors generated with SSR of the respective sensillum. Inset is the name of the olfactory receptor, the number of applied odors, and the lifetime sparseness, *S*. Color code refers to Figure 1B. Raw SSR data are listed in Table S3.

(B) Bar plot representing the lifetime sparseness for all olfactory receptor types.

(C) Scatterplots showing the correlation of the lifetime sparseness with number of OSNs (left), the number of PNs (middle), and the LN innervation frequency (right) per glomerulus. *p < 0.05 (two-tailed probability of the Pearson correlation coefficient).

Vosshall, 2005; Kurtovic et al., 2007; Silbering et al., 2011). The total number of sensilla per class corresponds to previously published reports and confirms that trichoid and basiconic sensilla are sexually dimorphic (Shanbhag et al., 1999; Stocker, 2001). We observed sexual dimorphism at the periphery of six sensillum types; these in turn comprise 18 olfactory receptor types. These types include olfactory receptors that are involved in courtship and mating (Or47b/Or88a/Or65a; Dweck et al., 2015; Lebreton et al., 2014), attraction behavior (Or83c; Ronderos et al., 2014), and CO_2 avoidance (Gr21a; Suh et al., 2004). Sexual dimorphism in the brain has been studied only at the glomerular level and not at the level of individual olfactory receptor types expressed in the

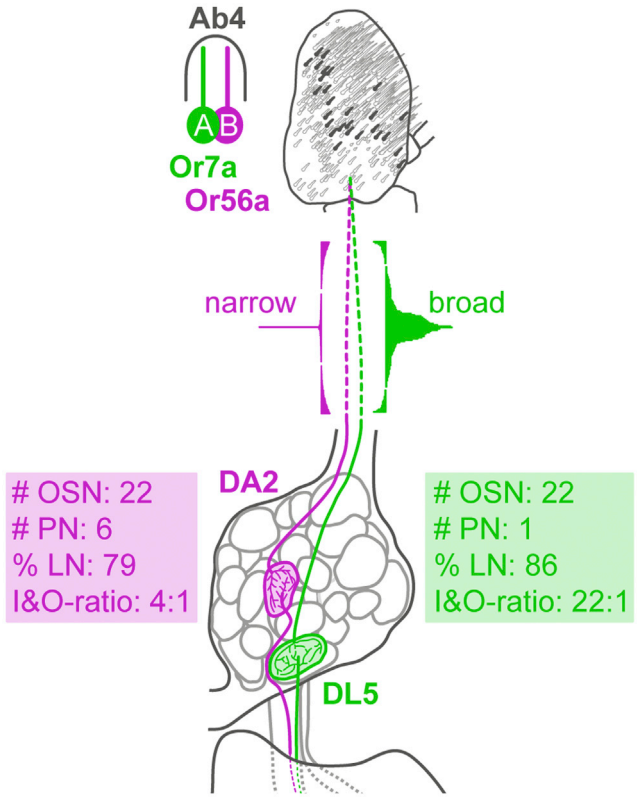

Figure 6. Glomerular Neuronal Architecture Reflects Functional Relevance

Schematic model displaying the morphological properties of two selected olfactory receptor pathways, Or56a/DA2 and Or7a/DL5, both of which descend from the Ab4 sensillum. The peripheral distribution of their sensilla over the odor response profile to their glomerular volume, convergence ratio, and LN innervation frequency (after Chou et al., 2010) are indicated. The color code refers to Figure 1B.

olfactory organs. Hence, our study demonstrates that the number of OSNs expressing a certain olfactory receptor type is different between the sexes, suggesting that those receptors might be involved in sex-specific behavior, such as courtship or oviposition. When we compared the female AL with the male AL, our data exceeded the number of dimorphic glomeruli described to date. Our data confirm that sexual dimorphism exists in the volumes of glomeruli DA1 and VA1v (Kondoh et al., 2003; Stockinger et al., 2005). We also agree that spatially adjacent glomeruli VA1d and DL3 are the same size in both sexes. We did not observe, however, that glomerulus VL2a is larger in males than in females, as it has been described (Stockinger et al., 2005), possibly because of the slight difference. In contrast to previous studies, we found sexual dimorphism in seven additional glomeruli, all of which are *fruitless* negative (Stockinger et al., 2005). These discrepancies might have a methodological basis. Although we quantified AL morphology under in vivo conditions, former studies analyzed glomerular volumes in brains that had been processed in vitro (Kondoh et al., 2003; Stockinger et al., 2005); such methodological disparities may cause unequal and unpredictable fixation artifacts in glomerular volume (Grabe et al., 2015). Our findings of additional, *fruitless* negative glomeruli with sex-specific volume differences suggest that other, so far unknown, factors might be involved. Future studies are needed to analyze whether these seven glomeruli are indeed involved in gender-specific behavior.

We observed that the majority of glomeruli is innervated by on average two uniglomerular PNs, while a few glomeruli relay their output via, on average, six uniglomerular PNs to higher brain centers. Our count of the number of PNs complements the previously published single cell clones of GH146-positive PNs (Jefferis et al., 2007; Marin et al., 2002, 2005; Wong et al., 2002) and confirms the estimated count of one to three uniglomerular PNs for most glomeruli (Wong et al., 2002). Notably, those glomeruli that exhibit the narrowest response profile seem to be innervated by the larger number of output neurons. These glomeruli are part of crucial pathways involved in reproduction and survival. For example, glomeruli DA1, VA1v, and VA1d are known to play a role in courtship and mating (Dweck et al., 2015; Kurtovic et al., 2007; Stockinger et al., 2005), while glomerulus DC3 is narrowly tuned to farnesol and mediates attraction behavior (Ronderos et al., 2014). Glomerulus DA2 encodes geosmin, the odor of toxic bacteria and mold, and evokes strong aversion in flies (Stensmyr et al., 2012). Glomerulus DL3 has so far not been deorphanized and will most likely have a very selected and narrow response profile. The olfactory system might therefore have evolved a strategy to ensure that highly essential odor cues are transferred reliably and quickly from the AL to higher brain centers. Indeed, it has recently been shown that higher PN numbers improve the detection accuracy and latency of odor stimuli (Jeanne and Wilson, 2015). In addition, large numbers of PNs might have the advantage of encoding diverse stimulus features, such as different intensities as suggested for the CO_2-encoding circuitry (Lin et al., 2013). We also demonstrate that narrowly tuned glomeruli are less frequently innervated by LNs, indicating that those glomeruli may be less integrated in the mainly inhibitory, interglomerular AL network than are broadly tuned glomeruli. This finding further underlines a straight feedforward network, ensuring fast processing and detection of key odorants. However, it must be kept in mind that the populations of OSNs, LNs, and PNs are not equal regarding their temporal response kinetics (Chou et al., 2010; de Bruyne et al., 2001; Laurent et al., 2001; Seki et al., 2010; Wilson et al., 2004). Hence, the final response of a glomerulus might not depend solely on neuron number but could be affected also by neuron-specific response dynamics.

Our main findings can be illustrated in the following representative example (Figure 6): glomeruli DL5 and DA2 receive input from 22 OSNs housed in the same basiconic sensillum type Ab4. The broad response profile of Or7a, whose OSNs target DL5 (Galizia et al., 2010), and the highly selective profile of Or56a targeting glomerulus DA2 and detecting geosmin (Stensmyr et al., 2012) represent two opposing input channels. DL5 is so far not affiliated with a specific behavioral task and seems to play a role in combinatorial coding of aversive odors (Knaden et al., 2012). The significance of glomerulus DA2 is supported by its high number of uniglomerular PNs, having potentially more random input sites on mushroom body Kenyon cells

(Caron et al., 2013; Gruntman and Turner, 2013) and on third-order neurons in the LH, in contrast to glomerulus DL5, which has only a single PN. The difference in output quantity is linked to an inverse LN innervation frequency. Although glomerulus DA2 is innervated by fewer LNs than is DL5, both glomeruli most likely have different impacts on the AL network. These glomeruli have different volumes, which, although the overall OSN density per glomerulus is identical, might be due either to the different number of innervating LNs or to a differential density of synapses per OSN (Mosca and Luo, 2014). On the basis of our findings of a specific and heterogeneous glomerular architecture, we are in a position to speculate about the significance of glomeruli that have remained to date poorly characterized. Hence, we propose that glomeruli D (Or69a), DC3 (Or83c), and DL3 (Or65a) likely encode odor information that is as crucial as information encoded in the geosmin and pheromone pathways.

In conclusion, our study demonstrates that each glomerulus is a unique morphological and functional unit whose significance regarding odor detection and odor-guided behavior can be predicted. Future studies dedicated to elucidating the synaptic connectivity in more detail will reveal whether ultrastructural characteristics of individual glomeruli are also correlated with functional properties.

EXPERIMENTAL PROCEDURES

Flies

Flies were reared at 25°C and 70% humidity on a 12 hr/12 hr day/night cycle. We used the following fly lines ordered from the Bloomington *Drosophila* stock center (http://flystocks.bio.indiana.edu): *GH146-GAL4* (Stocker et al., 1997), *UAS-GCaMP3.0* (Tian et al., 2009), *UAS-nlsGFP*, *ChA-GAL4* (Salvaterra and Kitamoto, 2001), *Or10a-GAL4*, *Or13a-GAL4*, *Or22a-GAL4*, *Or33c-GAL4*, *Or35a-GAL4*, *Or42a-GAL4*, *Or42b-GAL4*, *Or43a-GAL4*, *Or43b-GAL4*, *Or46aA-GAL4*, *Or47a-GAL4*, *Or49a-GAL4*, *Or56a-GAL4*, *Or59c-GAL4*, *Or67c-GAL4*, *Or69a-GAL4*, *Or83c-GAL4*, *Or85a-GAL4*, *Or88a-GAL4*, *Or92a-GAL4*, *Or98a-GAL4*, and *Orco-GAL4* (all Fishilevich and Vosshall, 2005; Vosshall et al., 2000). Additional lines were kindly provided by Richard Benton (*Ir40a-GAL4*; *Ir41a-GAL4*, Silbering et al., 2011; *IR76a-GAL4*, Benton et al., 2009; *Ir92a-GAL4*; and *Ir8a-GAL4*, Abuin et al., 2011), Barry Dickson (*Or67d-GAL4*, Kurtovic et al., 2007), and Bob Datta (*UAS-C3PA*; Ruta et al., 2010).

Scanning Electron Microscopy

Flies were anesthetized in CO_2, placed in 5 ml 25% EtOH, and incubated for 12–24 hr at room temperature. In an EtOH row, the flies were further dehydrated in 50%, 75%, and two times 100% EtOH for 12–24 hr each at room temperature. Samples were then critical point dried. After mounting the samples with T. V. tube coat (Ted Pella) onto the SEM stubs, we sputter-coated them with a 25-nm-thick platinum coat. Images of the sensillum types on the third antennal segment and the maxillary palp were acquired using a LEO 1450 VP scanning electron microscope with 10 kV and 24 mm working distance (Carl Zeiss).

OSN Quantification and Mapping

To quantify the number of OSNs innervating each glomerulus, 3- to 6-day-old flies were anesthetized with CO_2, and their antennae or palps were collected. After the antennae or palps were covered with a solution of saline and Triton-X (Sigma-Aldrich), they were mounted in VectaShield (Vector Laboratories) and sealed with nail polish between a 22 × 22 mm and a 24 × 60 mm object slide, both 1 mm thick, to allow double-sided scanning. No spacer was needed, because the layer of nail polish provided enough space to fix the antennae or palp but not crush it. Scans of both sides of each antenna were carried out with an Axio Imager.Z1 (Carl Zeiss) using a 20× water immersion objective (W Plan-Apochromat 20×/0.8; Carl Zeiss) in combination with a GFP filter cube (HE 38, EX BP 470/40, BS FT 495, EM BP 525/50; Carl Zeiss). To reliably map the sensilla, an additional transmitted light scan of each antenna was acquired. This scan was used to register all antennae by hand, on the basis of the position of the arista and the sacculus. The quantification of OSN cell bodies was done in FIJI (ImageJ version 1.48r; NIH) software.

Confocal Microscopy, 3D Reconstruction, and Volume Quantification

The dissection of fly brains was carried out as previously described (Silbering et al., 2011; Strutz et al., 2012). Confocal scans were obtained using multiple-photon confocal laser scanning microscopy (MPCLSM) (Zeiss laser scanning microscopy [LSM] 710 NLO confocal microscope; Carl Zeiss) using a 40× water immersion objective (W Plan-Apochromat 40x/1.0 DIC M27; Carl Zeiss) in combination with the internal Argon 488 (LASOS) and Helium-Neon 543 (Carl Zeiss) laser lines. Reconstruction of whole ALs and of individual glomeruli was done using the segmentation software AMIRA version 5.5.0 (FEI Visualization Sciences Group). Identification of glomeruli was verified by the in vivo scans of the specific OR-lines crossed into the END1-2 background for in vivo neuropil labeling (Grabe et al., 2015). We analyzed scans of at least three specimens for each GAL4 receptor line and reconstructed them in using the segmentation software AMIRA 5.5.0 (FEI Visualization Sciences Group). Using information on the voxel size from the laser scanning microscopy scans as well as the number of voxels labeled for each neuropil in AMIRA, we calculated the volume of the glomeruli and the whole AL.

Photoactivation of PNs

In vivo labeling of single glomeruli of 4- to 6-day-old male and female flies of the genotype *+;GH146-GAL4/(CyO);UAS-C3PA/(TM6B)* using MPCLSM (Zeiss LSM 710 NLO confocal microscope; Carl Zeiss) equipped with an infrared Chameleon Ultra diode-pumped laser (Coherent). Flies were prepared as previously described (Strutz et al., 2012). Precise regions of interest (ROIs) in the center of each single glomerulus were continuously photoactivated for 5–15 min at a wavelength of 760 nm with a 40× water immersion objective (W Plan-Apochromat 40x/1.0 DIC M27; Carl Zeiss) with laser power of approximately 1.5 mW. In detail, after obtaining a pre-photoactivation scan of the whole AL, we identified the single target glomerulus, marked its volume with a precise ROI, photoactivated and subsequently labeled all GH146-positive PNs innervating it, including all corresponding somata in one of the three cell clusters surrounding the AL (Figure 3A) as well as all axonal projections to the mushroom body calyx and the LH. Z stacks of the pre- and post-activation states were scanned at 925 nm with 1,024 × 1,024 pixel resolution. The identification of glomeruli was based on the previously published screen of *GH146-GAL4/UAS-GCaMP3.0* under the same conditions (Grabe et al., 2015).

Single-Sensillum Recordings

Adult flies were immobilized in pipette tips, and the third antennal segment or the palps were placed in a stable position onto a glass coverslip. Sensilla were localized under a microscope (BX51WI; Olympus) at 100× magnification, and the extracellular signals originating from the OSNs were measured by inserting a tungsten wire electrode in the base of a sensillum. The reference electrode was inserted into the eye. Signals were amplified (10×; Syntech Universal AC/DC Probe; Syntech), sampled (10,667.0 samples/s), and filtered (100–3,000 Hz with 50/60 Hz suppression) via USB-IDAC connection to a computer (Syntech). Action potentials were extracted using Auto Spike 32 software (Syntech). Neuron activities were recorded for 10 s, starting 2 s before a stimulation period of 0.5 s. Responses from individual neurons were calculated as the increase (or decrease) in the action potential frequency (spikes per second) relative to the pre-stimulus frequency.

Lifetime Sparseness, *S*

Acquired responses were used to quantify a receptor's response profile by calculating its lifetime sparseness (Bhandawat et al., 2007; Perez-Orive et al., 2002; Vinje and Gallant, 2000). This is a non-parametric statistic providing a measure of the likeliness of an OSN to respond. The value ranges from $0 \leq S \leq 1$, where 0 means the OSN responds to every odor in the same

way and 1 means the OSN responds exclusively to one odor in the set. Calculation was carried out with following formula:

$$S = \left(\frac{1}{1-\frac{1}{N}}\right) * \left(1 - \frac{\left(\sum_{j=1}^{N} \frac{r_j}{N}\right)^2}{\sum_{j=1}^{N} \frac{r_j^2}{N}}\right),$$

where S is lifetime sparseness, N is the number of tested odors, and r_j is response to a given odor j. Any values of $r_j < 0$ were set to zero before computing lifetime sparseness. Used data sets are taken from Dweck et al. (2015), Ebrahim et al. (2015), and Hallem and Carlson (2006); the DoOR database (Galizia et al., 2010), and response profiles of 11 olfactory receptors acquired via SSR in this study (Table S3).

Statistical Methods

If not otherwise stated, data represent median ± SD. Statistical differences between groups were determined by Student's t test (*$p < 0.05$, **$p < 0.01$, ***$p < 0.001$).

Significance of the Pearson correlation coefficients were calculated using the online tool p-Value Calculator for Correlation Coefficients (http://www.danielsoper.com/statcalc).

SUPPLEMENTAL INFORMATION

Supplemental Information includes one figure and three tables and can be found with this article online at http://dx.doi.org/10.1016/j.celrep.2016.08.063.

AUTHOR CONTRIBUTIONS

V.G. and S.S. together conceived and designed the study. V.G. planned and carried out all experiments, with the exception of the quantification of PNs in females (Figure 3), which was done by A.B., and the SSR experiments (Figure 5), which were done by H.K.M.D. V.G. and S.S. analyzed and interpreted the results, prepared the figures, and wrote the paper. S.L.-L. helped to generate the END1-2 fly strain and provided neurogenetic advice. B.S.H. provided intellectual and financial support. All authors critically revised the article.

ACKNOWLEDGMENTS

We thank Silke Trautheim for excellent technical assistance, Jürgen Rybak for help with the AMIRA software, Christine Mißbach for support regarding the antennal preparations, Carolin Kathner and Julia van Beesel for help with the neuronal quantifications, and Emily Wheeler for editorial assistance. Stocks obtained from the Bloomington Drosophila Stock Center (NIH P40OD018537) were used in this study. We are grateful to the Hansson Department for comments on the manuscript. This study was funded by the Federal Ministry of Education and Research (BMBF research grant to S.S.) and the Max Planck Society (MPG).

Received: March 26, 2016
Revised: July 15, 2016
Accepted: August 18, 2016
Published: September 20, 2016

REFERENCES

Abuin, L., Bargeton, B., Ulbrich, M.H., Isacoff, E.Y., Kellenberger, S., and Benton, R. (2011). Functional architecture of olfactory ionotropic glutamate receptors. Neuron *69*, 44–60.

Acebes, A., and Ferrús, A. (2001). Increasing the number of synapses modifies olfactory perception in Drosophila. J. Neurosci. *21*, 6264–6273.

Ai, M., Min, S., Grosjean, Y., Leblanc, C., Bell, R., Benton, R., and Suh, G.S.B. (2010). Acid sensing by the Drosophila olfactory system. Nature *468*, 691–695.

Benton, R., Sachse, S., Michnick, S.W., and Vosshall, L.B. (2006). Atypical membrane topology and heteromeric function of *Drosophila* odorant receptors *in vivo*. PLoS Biol. *4*, e20.

Benton, R., Vannice, K.S., Gomez-Diaz, C., and Vosshall, L.B. (2009). Variant ionotropic glutamate receptors as chemosensory receptors in Drosophila. Cell *136*, 149–162.

Bhandawat, V., Olsen, S.R., Gouwens, N.W., Schlief, M.L., and Wilson, R.I. (2007). Sensory processing in the Drosophila antennal lobe increases reliability and separability of ensemble odor representations. Nat. Neurosci. *10*, 1474–1482.

Boeckh, J., and Tolbert, L.P. (1993). Synaptic organization and development of the antennal lobe in insects. Microsc. Res. Tech. *24*, 260–280.

Bressel, O.C., Khan, M., and Mombaerts, P. (2016). Linear correlation between the number of olfactory sensory neurons expressing a given mouse odorant receptor gene and the total volume of the corresponding glomeruli in the olfactory bulb. J. Comp. Neurol. *524*, 199–209.

Busch, S., Selcho, M., Ito, K., and Tanimoto, H. (2009). A map of octopaminergic neurons in the Drosophila brain. J. Comp. Neurol. *513*, 643–667.

Carlsson, M.A., Diesner, M., Schachtner, J., and Nässel, D.R. (2010). Multiple neuropeptides in the Drosophila antennal lobe suggest complex modulatory circuits. J. Comp. Neurol. *518*, 3359–3380.

Caron, S.J.C., Ruta, V., Abbott, L.F., and Axel, R. (2013). Random convergence of olfactory inputs in the Drosophila mushroom body. Nature *497*, 113–117.

Chou, Y.-H., Spletter, M.L., Yaksi, E., Leong, J.C.S., Wilson, R.I., and Luo, L. (2010). Diversity and wiring variability of olfactory local interneurons in the Drosophila antennal lobe. Nat. Neurosci. *13*, 439–449.

Couto, A., Alenius, M., and Dickson, B.J. (2005). Molecular, anatomical, and functional organization of the *Drosophila* olfactory system. Curr. Biol. *15*, 1535–1547.

de Bruyne, M., Clyne, P.J., and Carlson, J.R. (1999). Odor coding in a model olfactory organ: the *Drosophila* maxillary palp. J. Neurosci. *19*, 4520–4532.

de Bruyne, M., Foster, K., and Carlson, J.R. (2001). Odor coding in the *Drosophila* antenna. Neuron *30*, 537–552.

Dekker, T., Ibba, I., Siju, K.P., Stensmyr, M.C., and Hansson, B.S. (2006). Olfactory shifts parallel superspecialism for toxic fruit in Drosophila melanogaster sibling, D. sechellia. Curr. Biol. *16*, 101–109.

Dobritsa, A.A., van der Goes van Naters, W., Warr, C.G., Steinbrecht, R.A., and Carlson, J.R. (2003). Integrating the molecular and cellular basis of odor coding in the *Drosophila* antenna. Neuron *37*, 827–841.

Duménil, C., Woud, D., Pinto, F., Alkema, J.T., Jansen, I., Van Der Geest, A.M., Roessingh, S., and Billeter, J.-C. (2016). Pheromonal cues deposited by mated females convey social information about egg-laying sites in Drosophila melanogaster. J. Chem. Ecol. *42*, 259–269.

Dweck, H.K., Ebrahim, S.A., Kromann, S., Bown, D., Hillbur, Y., Sachse, S., Hansson, B.S., and Stensmyr, M.C. (2013). Olfactory preference for egg laying on citrus substrates in Drosophila. Curr. Biol. *23*, 2472–2480.

Dweck, H.K.M., Ebrahim, S.A.M., Thoma, M., Mohamed, A.A.M., Keesey, I.W., Trona, F., Lavista-Llanos, S., Svatoš, A., Sachse, S., Knaden, M., and Hansson, B.S. (2015). Pheromones mediating copulation and attraction in Drosophila. Proc. Natl. Acad. Sci. U S A *112*, E2829–E2835.

Ebrahim, S.A.M., Dweck, H.K.M., Stökl, J., Hofferberth, J.E., Trona, F., Weniger, K., Rybak, J., Seki, Y., Stensmyr, M.C., Sachse, S., et al. (2015). *Drosophila* avoids parasitoids by sensing their semiochemicals via a dedicated olfactory circuit. PLoS Biol. *13*, e1002318.

Fishilevich, E., and Vosshall, L.B. (2005). Genetic and functional subdivision of the *Drosophila* antennal lobe. Curr. Biol. *15*, 1548–1553.

Galizia, C.G., McIlwrath, S.L., and Menzel, R. (1999). A digital three-dimensional atlas of the honeybee antennal lobe based on optical sections acquired by confocal microscopy. Cell Tissue Res. *295*, 383–394.

Galizia, C.G., Münch, D., Strauch, M., Nissler, A., and Ma, S. (2010). Integrating heterogeneous odor response data into a common response model: a DoOR to the complete olfactome. Chem. Senses *35*, 551–563.

Gallio, M., Ofstad, T.A., Macpherson, L.J., Wang, J.W., and Zuker, C.S. (2011). The coding of temperature in the Drosophila brain. Cell *144*, 614–624.

Gao, Q., Yuan, B., and Chess, A. (2000). Convergent projections of *Drosophila* olfactory neurons to specific glomeruli in the antennal lobe. Nat. Neurosci. *3*, 780–785.

Grabe, V., Strutz, A., Baschwitz, A., Hansson, B.S., and Sachse, S. (2015). Digital in vivo 3D atlas of the antennal lobe of Drosophila melanogaster. J. Comp. Neurol. *523*, 530–544.

Grosjean, Y., Rytz, R., Farine, J.-P., Abuin, L., Cortot, J., Jefferis, G.S.X.E., and Benton, R. (2011). An olfactory receptor for food-derived odours promotes male courtship in Drosophila. Nature *478*, 236–240.

Gruntman, E., and Turner, G.C. (2013). Integration of the olfactory code across dendritic claws of single mushroom body neurons. Nat. Neurosci. *16*, 1821–1829.

Ha, T.S., and Smith, D.P. (2006). A pheromone receptor mediates 11-cis-vaccenyl acetate-induced responses in *Drosophila*. J. Neurosci. *26*, 8727–8733.

Hallem, E.A., and Carlson, J.R. (2006). Coding of odors by a receptor repertoire. Cell *125*, 143–160.

Hansson, B.S., Ljungberg, H., Hallberg, E., and Löfstedt, C. (1992). Functional specialization of olfactory glomeruli in a moth. Science *256*, 1313–1315.

Hansson, B.S., Knaden, M., Sachse, S., Stensmyr, M.C., and Wicher, D. (2010). Towards plant-odor-related olfactory neuroethology in *Drosophila*. Chemoecology *20*, 51–61.

Hong, E.J., and Wilson, R.I. (2015). Simultaneous encoding of odors by channels with diverse sensitivity to inhibition. Neuron *85*, 573–589.

Ito, K., Shinomiya, K., Ito, M., Armstrong, J.D., Boyan, G., Hartenstein, V., Harzsch, S., Heisenberg, M., Homberg, U., Jenett, A., et al.; Insect Brain Name Working Group (2014). A systematic nomenclature for the insect brain. Neuron *81*, 755–765.

Jeanne, J.M., and Wilson, R.I. (2015). Convergence, divergence, and reconvergence in a feedforward network improves neural speed and accuracy. Neuron *88*, 1014–1026.

Jefferis, G.S.X.E., Potter, C.J., Chan, A.M., Marin, E.C., Rohlfing, T., Maurer, C.R., Jr., and Luo, L. (2007). Comprehensive maps of Drosophila higher olfactory centers: spatially segregated fruit and pheromone representation. Cell *128*, 1187–1203.

Kain, P., Boyle, S.M., Tharadra, S.K., Guda, T., Pham, C., Dahanukar, A., and Ray, A. (2013). Odour receptors and neurons for DEET and new insect repellents. Nature *502*, 507–512.

Knaden, M., Strutz, A., Ahsan, J., Sachse, S., and Hansson, B.S. (2012). Spatial representation of odorant valence in an insect brain. Cell Rep. *1*, 392–399.

Kondoh, Y., Kaneshiro, K.Y., Kimura, K., and Yamamoto, D. (2003). Evolution of sexual dimorphism in the olfactory brain of Hawaiian *Drosophila*. Proc. Biol. Sci. *270*, 1005–1013.

Kreher, S.A., Mathew, D., Kim, J., and Carlson, J.R. (2008). Translation of sensory input into behavioral output via an olfactory system. Neuron *59*, 110–124.

Kurtovic, A., Widmer, A., and Dickson, B.J. (2007). A single class of olfactory neurons mediates behavioural responses to a Drosophila sex pheromone. Nature *446*, 542–546.

Lai, S.-L., Awasaki, T., Ito, K., and Lee, T. (2008). Clonal analysis of Drosophila antennal lobe neurons: diverse neuronal architectures in the lateral neuroblast lineage. Development *135*, 2883–2893.

Laissue, P.P., Reiter, C., Hiesinger, P.R., Halter, S., Fischbach, K.F., and Stocker, R.F. (1999). Three-dimensional reconstruction of the antennal lobe in *Drosophila melanogaster*. J. Comp. Neurol. *405*, 543–552.

Larsson, M.C., Domingos, A.I., Jones, W.D., Chiappe, M.E., Amrein, H., and Vosshall, L.B. (2004). *Or83b* encodes a broadly expressed odorant receptor essential for *Drosophila* olfaction. Neuron *43*, 703–714.

Laurent, G., Stopfer, M., Friedrich, R.W., Rabinovich, M.I., Volkovskii, A., and Abarbanel, H.D.I. (2001). Odor encoding as an active, dynamical process: experiments, computation, and theory. Annu. Rev. Neurosci. *24*, 263–297.

Lebreton, S., Grabe, V., Omondi, A.B., Ignell, R., Becher, P.G., Hansson, B.S., Sachse, S., and Witzgall, P. (2014). Love makes smell blind: mating suppresses pheromone attraction in Drosophila females via Or65a olfactory neurons. Sci. Rep. *4*, 7119.

Lin, H.-H., Chu, L.-A., Fu, T.-F., Dickson, B.J., and Chiang, A.-S. (2013). Parallel neural pathways mediate CO_2 avoidance responses in Drosophila. Science *340*, 1338–1341.

Linz, J., Baschwitz, A., Strutz, A., Dweck, H.K.M., Sachse, S., Hansson, B.S., and Stensmyr, M.C. (2013). Host plant-driven sensory specialization in Drosophila erecta. Proc. Biol. Sci. *280*, 20130626.

Liu, W.W., and Wilson, R.I. (2013). Glutamate is an inhibitory neurotransmitter in the Drosophila olfactory system. Proc. Natl. Acad. Sci. U S A *110*, 10294–10299.

Marin, E.C., Jefferis, G.S.X.E., Komiyama, T., Zhu, H., and Luo, L. (2002). Representation of the glomerular olfactory map in the Drosophila brain. Cell *109*, 243–255.

Marin, E.C., Watts, R.J., Tanaka, N.K., Ito, K., and Luo, L. (2005). Developmentally programmed remodeling of the Drosophila olfactory circuit. Development *132*, 725–737.

Mombaerts, P. (2006). Axonal wiring in the mouse olfactory system. Annu. Rev. Cell Dev. Biol. *22*, 713–737.

Mosca, T.J., and Luo, L. (2014). Synaptic organization of the Drosophila antennal lobe and its regulation by the Teneurins. Elife *3*, e03726.

Patterson, G.H., and Lippincott-Schwartz, J. (2002). A photoactivatable GFP for selective photolabeling of proteins and cells. Science *297*, 1873–1877.

Perez-Orive, J., Mazor, O., Turner, G.C., Cassenaer, S., Wilson, R.I., and Laurent, G. (2002). Oscillations and sparsening of odor representations in the mushroom body. Science *297*, 359–365.

Ronderos, D.S., Lin, C.-C., Potter, C.J., and Smith, D.P. (2014). Farnesol-detecting olfactory neurons in Drosophila. J. Neurosci. *34*, 3959–3968.

Ruta, V., Datta, S.R., Vasconcelos, M.L., Freeland, J., Looger, L.L., and Axel, R. (2010). A dimorphic pheromone circuit in Drosophila from sensory input to descending output. Nature *468*, 686–690.

Rybak, J., Talarico, G., Ruiz, S., Arnold, C., Cantera, R., and Hansson, B.S. (2016). Synaptic circuitry of identified neurons in the antennal lobe of Drosophila melanogaster. J. Comp. Neurol. *524*, 1920–1956.

Sachse, S., Rueckert, E., Keller, A., Okada, R., Tanaka, N.K., Ito, K., and Vosshall, L.B. (2007). Activity-dependent plasticity in an olfactory circuit. Neuron *56*, 838–850.

Salvaterra, P.M., and Kitamoto, T. (2001). Drosophila cholinergic neurons and processes visualized with Gal4/UAS-GFP. Brain Res. Gene Expr. Patterns *1*, 73–82.

Schneiderman, A.M., Hildebrand, J.G., Brennan, M.M., and Tumlinson, J.H. (1986). Trans-sexually grafted antennae alter pheromone-directed behaviour in a moth. Nature *323*, 801–803.

Seki, Y., Rybak, J., Wicher, D., Sachse, S., and Hansson, B.S. (2010). Physiological and morphological characterization of local interneurons in the Drosophila antennal lobe. J. Neurophysiol. *104*, 1007–1019.

Semmelhack, J.L., and Wang, J.W. (2009). Select Drosophila glomeruli mediate innate olfactory attraction and aversion. Nature *459*, 218–223.

Shanbhag, S.R., Singh, K., and Singh, R.N. (1995). Fine structure and primary sensory projections of sensilla located in the sacculus of the antenna of Drosophila melanogaster. Cell Tissue Res. *282*, 237–249.

Shanbhag, S.R., Muller, B., and Steinbrecht, R.A. (1999). Atlas of olfactory organs of *Drosophila melanogaster*. 1. Types, external organization, innervation and distribution of olfactory sensilla. Int. J. Insect Morphol. Embryol. *28*, 377–397.

Shang, Y., Claridge-Chang, A., Sjulson, L., Pypaert, M., and Miesenböck, G. (2007). Excitatory local circuits and their implications for olfactory processing in the fly antennal lobe. Cell *128*, 601–612.

Silbering, A.F., Rytz, R., Grosjean, Y., Abuin, L., Ramdya, P., Jefferis, G.S.X.E., and Benton, R. (2011). Complementary function and integrated wiring of the evolutionarily distinct Drosophila olfactory subsystems. J. Neurosci. *31*, 13357–13375.

Stensmyr, M.C., Dweck, H.K.M., Farhan, A., Ibba, I., Strutz, A., Mukunda, L., Linz, J., Grabe, V., Steck, K., Lavista-Llanos, S., et al. (2012). A conserved dedicated olfactory circuit for detecting harmful microbes in Drosophila. Cell *151*, 1345–1357.

Stocker, R.F. (2001). *Drosophila* as a focus in olfactory research: mapping of olfactory sensilla by fine structure, odor specificity, odorant receptor expression, and central connectivity. Microsc. Res. Tech. *55*, 284–296.

Stocker, R.F., Lienhard, M.C., Borst, A., and Fischbach, K.F. (1990). Neuronal architecture of the antennal lobe in *Drosophila melanogaster*. Cell Tissue Res. *262*, 9–34.

Stocker, R.F., Heimbeck, G., Gendre, N., and de Belle, J.S. (1997). Neuroblast ablation in *Drosophila* P[GAL4] lines reveals origins of olfactory interneurons. J. Neurobiol. *32*, 443–456.

Stockinger, P., Kvitsiani, D., Rotkopf, S., Tirián, L., and Dickson, B.J. (2005). Neural circuitry that governs Drosophila male courtship behavior. Cell *121*, 795–807.

Strausfeld, N.J., and Hildebrand, J.G. (1999). Olfactory systems: common design, uncommon origins? Curr. Opin. Neurobiol. *9*, 634–639.

Strutz, A., Voeller, T., Riemensperger, T., Fiala, A., and Sachse, S. (2012). Calcium imaging of neural activity in the olfactory system of Drosophila. In Genetically Encoded Functional Indicators, J.-R. Martin, ed. (Springer Science+Business Media), pp. 43–70.

Suh, G.S., Wong, A.M., Hergarden, A.C., Wang, J.W., Simon, A.F., Benzer, S., Axel, R., and Anderson, D.J. (2004). A single population of olfactory sensory neurons mediates an innate avoidance behaviour in *Drosophila*. Nature *431*, 854–859.

Tian, L., Hires, S.A., Mao, T., Huber, D., Chiappe, M.E., Chalasani, S.H., Petreanu, L., Akerboom, J., McKinney, S.A., Schreiter, E.R., et al. (2009). Imaging neural activity in worms, flies and mice with improved GCaMP calcium indicators. Nat. Methods *6*, 875–881.

Vinje, W.E., and Gallant, J.L. (2000). Sparse coding and decorrelation in primary visual cortex during natural vision. Science *287*, 1273–1276.

Vosshall, L.B., and Stocker, R.F. (2007). Molecular architecture of smell and taste in Drosophila. Annu. Rev. Neurosci. *30*, 505–533.

Vosshall, L.B., Wong, A.M., and Axel, R. (2000). An olfactory sensory map in the fly brain. Cell *102*, 147–159.

Wilson, R.I. (2013). Early olfactory processing in Drosophila: mechanisms and principles. Annu. Rev. Neurosci. *36*, 217–241.

Wilson, R.I., and Mainen, Z.F. (2006). Early events in olfactory processing. Annu. Rev. Neurosci. *29*, 163–201.

Wilson, R.I., Turner, G.C., and Laurent, G. (2004). Transformation of olfactory representations in the *Drosophila* antennal lobe. Science *303*, 366–370.

Wong, A.M., Wang, J.W., and Axel, R. (2002). Spatial representation of the glomerular map in the *Drosophila* protocerebrum. Cell *109*, 229–241.